Proceedings of IMECE2006
2006 ASME International Mechanical Engineering Congress and Exposition
November 5-10, 2006, Chicago, Illinois, USA

IMECE2006-14889

COMPARISON OF EXPERIMENTAL AND NUMERICAL TEMPERATURE DISTRIBUTIONS IN TISSUES DURING SHORT PULSE LASER IRRADIATION USING FOCUSED BEAM

Ashim Dutta[1] **Gopalendu Pal**[1] **Kunal Mitra**[1] **Michael S. Grace**[2]
[1] Mechanical and Aerospace Engineering Department
[2] Department of Biological Sciences
Florida Institute of Technology
Melbourne, FL 32901

ABSTRACT

The objective of this work is to perform experimental measurements validated with numerical modeling results for analyzing the temperature distributions and heat affected zone during short pulse laser irradiation of tissues using focused beam. A Q-switched laser is used as a radiation source. A three-layered tissue phantom model of skin consisting of epidermis, dermis, and fatty tissues is first considered for model validation. Tumors are simulated with inhomogeneities embedded inside the tissue phantoms. Experiments are next conducted with freshly excised skin tissue samples from mice and finally on live anaesthetized mice to consider the bulk effect of convective heat transfer due to blood flow. Experimental measurements of axial and radial temperature distributions for all the cases are compared with numerical modeling results obtained using Pennes' bio-heat transfer equation coupled with either traditional Fourier parabolic or non-Fourier hyperbolic heat conduction formulation. Experimentally measured temperature profiles in tissue phantoms, skin tissue samples, and live anaesthetized mice are found to match extremely well with the predictions from the non-Fourier model than the Fourier formulation by considering skin as a multi-layered medium. It is also observed that focused laser beam produces desired temperature rise at the target site with lesser radial spread compared to a collimated laser beam source.

INTRODUCTION

In recent years, therapeutic applications using short pulse laser energy source have become popular due to controllability in energy input, precision in achievement of heat affected zone, and minimally invasive nature of the treatment procedures. Short pulse lasers are extensively used in therapeutic applications, such as photodynamic treatment of port-wine stains [1], selective photothermolysis [2], tumor irradiation [3-7], fractional photothermolysis and non-ablative dermal remodeling [8, 9], laser vascular treatment [10, 11] and treatment of muscles [12].

The ability to produce highly localized heating at the desired position leading to minimal collateral damage to the surrounding tissues made short pulse laser an obvious choice for therapeutic application, such as tumor irradiation. It has been well established that a temperature rise of around 43°C is required at the tumor location for successful tumor irradiation without damaging adjacent healthy tissue [13, 14]. In order to achieve desired temperature rise and localized heat affected zone for successful tumor irradiation, proper energy delivery technique to the target site is necessary. Traditionally tumor irradiation has been performed using collimated beam in two ways: direct delivery for tumors close to the skin surface [4] and fiber-optic delivery for tumors seated deep inside the body [5, 7, 15]. The potential disadvantage of collimated irradiation is the development of large heat affected zone surrounding the spot of irradiation along with low temperature rise at the centre of the spot. This shortcoming can be eliminated successfully by using a focused laser beam delivered directly at the tumor site using converging lens. Although focused beam has been used in applications, such as fractional photothermolysis [8], non-ablative skin remodeling [9], and treatment of striated muscles [12] involving treatment zone underneath the skin surface, no study has been reported in the literature involving focused laser beam for tumor irradiation application.

During laser irradiation of tissues, a detailed understanding of bio-heat transfer phenomenon is required to ensure accurate and controlled deposition of energy into the desired location with minimum collateral thermal damage to adjoining healthy tissues. Substantial efforts have been made previously to develop a complete theoretical model considering the inherent complexity of the heat transfer process coupled with blood perfusion phenomenon in tissue medium. Among various models developed, two basic and widely accepted models which consider the effect of blood perfusion on heat transport through tissues are Pennes' bio-heat transfer model [16] and Weinbaum and Jiji (WJ) model [17]. WJ bio-heat model indicates that blood-tissue heat transfer is dependent on the local vascular geometry and flow velocity, whereas Pennes' model takes into account the convective effects of the of the blood flow as an isotropic heat source or sink. Later Zhu et al [18] have modified WJ model by incorporating blood perfusion through microvessels of unequal size and studied the effect on

local average tissue temperature. Various other models have also been developed by modifying these two basic models for different blood vessel networks and local vascular geometries, e.g. a bio-heat transfer model has been developed by considering arrays of blood vessels and studying convective and perfusive modalities of heat transfer in living tissues [19, 20]. Other models have been developed by considering blood vessels in pairs and incorporating vessel to vessel heat transfer in tissue medium [21-23]. Several analytical and numerical studies have also been reported in the literature by considering blood perfusion effect using Pennes' model [24-26]. Pennes' energy balance model has been coupled with thermal wave model of bio-heat transfer [TWMBT] to numerically evaluate temperature history for the case of instantaneous heating of skin, such as burning due to flash fire [25]. Heat transfer within a perfused tissue in the presence of a blood vessel has been studied for the case of metabolic heat generation using Pennes' model [24]. It has been demonstrated that variable metabolic heat generation and variable blood perfusion gives more accurate description of the process of heat transfer inside the tissue medium [24]. Analytical solution of the bio-heat transfer problem has been developed using Pennes' 1-D energy balance equation [26]. Temperature history and spatial temperature profiles of tissue medium have been analyzed for different boundary conditions and energy source terms, such as constant, sinusoidal, step, point or stochastic heating [26]. Depending on the energy source term, all these above-mentioned works are focused on bio-heat transfer models in two main categories: one in which there is internal source of heat generation (i.e. metabolism) [16, 17, 20] and the other in which there is an external source of heat generation (such as laser irradiation) [27]. It has already been demonstrated that Penne's model is a good approximation of the tissue temperature profiles for laser irradiation of tissues [27].

Traditionally, Fourier heat conduction formulation has been used to account for the heat flux in both Pennes' and WJ bioheat model. In Fourier heat conduction formulation, it is assumed that heat wave travels with an infinite velocity in the medium. This assumption does not hold good in case of heat transfer in tissue at short time scales when heated by ephemeral heat source like lasers. Analysis of thermodynamics of such a phenomenon [28, 29] indicates a need to account for finite propagation speed of thermal wave through the medium. Hyperbolic heat conduction formulation incorporates this wave nature of thermal disturbance propagation by introducing a new parameter called thermal relaxation time. Hyperbolic heat conduction implies that a certain time is required for the heat flux to change the temperature gradient in the medium [30]. It has been demonstrated that thermal relaxation time has a strong effect in case of laser-tissue interaction at short time scale [31]. Thermal relaxation times of different porous materials have been experimentally measured and are reported in the literature [32, 33]. Temperature distribution and heat affected zone for the case of laser irradiated homogeneous tissue phantoms and bologna meat samples have also been measured experimentally and validated numerically using hyperbolic heat conduction formulation [34]. Recently, a new model named Dual Phase Lag (DPL) has been developed [35, 36] in which the wave like feature of hyperbolic heat conduction is considered along with diffusion. The DPL model accounts for deviations from classical approach by introducing the phase lags τ_q and τ_T of heat flux and temperature gradient, respectively [36].

The objective of this paper is to perform experimental and numerical analysis of the temperature distributions and heat affected zone during short pulse laser irradiation of tissues using focused laser beam. Skin is modeled as a three-layered medium having different optical properties in each layer. Experiments are performed on three-layered tissue phantom containing inhomogeneity simulating tumor. The phantom is irradiated by a Q-switched short pulse laser source focused directly at the inhomogeneity location using a converging lens. The effectiveness of using a focused beam rather than a collimated beam to obtain required temperature rise at the region of interest with smaller heat affected zone is demonstrated. The results of multi-layer tissue phantoms are also compared with those of a single-layer tissue phantom. After phantom validation studies experiments are conducted on freshly excised skin tissue samples from mice by irradiating the sample with different powers. Finally experiments are performed on live anaesthetized mice to account for the effect of blood perfusion on heat transfer through tissue medium during laser irradiation. The experimental results for all the cases considered are compared with the numerical results obtained from Pennes' bio-heat transfer model using both Fourier parabolic and non-Fourier hyperbolic heat conduction formulations.

NOMENCLATURE

C	specific heat of tissue
C_b	specific heat of blood
R_D	beam radius at the focal plane
R_o	beam radius at the sample surface
T	temperature
k_a	absorption coefficient of tissue
k_e	extinction coefficient of tissue
q	heat flux
r, z	spatial coordinates
t	time
t_p	pulse width of laser beam
$u(t)$	unit step function
α	thermal diffusivity of tissue
$\delta(t)$	Dirac delta function
κ	thermal conductivity of tissue
ρ	density of tissue
ρ_b	density of blood
τ	relaxation time
ω_b	blood perfusion rate

MATHEMATICAL FORMULATION

To study the temperature distribution and analyze the heat diffusion zone during laser irradiation of tissue medium, Pennes' energy equation is coupled with Fourier parabolic and non-Fourier hyperbolic heat conduction equation and the resulting equations are solved numerically. A pulsed laser beam of pulse width (t_p) is incident normally and focused on the sample at the zone of interest as shown in Fig. 1a. The laser beam has a Gaussian distribution in radial direction and hence an axi-symmetric cylindrical coordinate system is used to describe the geometry. The temporal distribution of the laser pulse is approximated with a rectangular profile.

Heat conduction through tissue medium is traditionally analyzed using Fourier heat conduction model which is given by:

$$q(r,z,t) = -\kappa \nabla T(r,z,t), \quad (1)$$

where T is the temperature, r and z are the spatial coordinates, t is the time, q is the heat flux, κ is the tissue thermal conductivity and ∇ is the gradient.

For laser tissue interaction incorporating scattering and absorption of laser energy in the tissue, the Pennes' energy equation which includes the convective effect due to blood perfusion can be written as:

$$-\nabla q(r,z,t) - \omega_b \rho_b C_b (T - T_a) + k_a L_0 \exp\left(\frac{-2r^2}{\sigma(z)^2}\right) \times \exp(-zk_e)[u(t) - u(t-t_p)] = \rho C \frac{\partial T}{\partial t}, \quad (2)$$

where T_a is the temperature of free stream velocity of blood flow which is taken as constant, ρ is the density of tissue, ρ_b is the density of blood, ω_b is blood perfusion rate, C is the specific heat of tissue, C_b is the specific heat of blood, $u(t)$ is the unit step function, L_o is the maximum intensity of the laser beam at the sample surface, k_a is the absorption coefficient, k_e is the extinction (scattering and absorption combined) coefficient, t_p is the laser pulse width, and $\sigma(z)$ is the standard deviation of radial intensity distribution varying with sample depth.

Eq. (1) and (2) are combined to obtain the parabolic diffusion equation whose solution implies an infinite speed of propagation of the thermal signal. To overcome the drawback of infinite speed of propagation of the thermal signal, a non-Fourier damped wave heat conduction model that takes into account finite speed of propagation of heat wave is considered and is given by [30-34]:

$$q(r,z,t) + \tau \frac{\partial q(r,z,t)}{\partial t} = -\kappa \nabla T(r,z,t), \quad (3)$$

where τ is the relaxation time of the medium. When the above non-Fourier relationship between heat flux and temperature is combined with the energy equation given by Eq. (2), the resultant equation is a hyperbolic non-Fourier partial differential equation as given by:

$$\frac{\partial^2 T}{\partial r^2} + \frac{1}{r}\frac{\partial T}{\partial r} + \frac{\partial^2 T}{\partial z^2} = \left[\frac{1}{\alpha} + \frac{\tau \omega_b \rho_b C_b}{\kappa}\right]\frac{\partial T}{\partial t} + \frac{\tau}{\alpha}\frac{\partial^2 T}{\partial t^2} + \omega_b \rho_b C_b (T - T_a) - \left\{ \left(1 + \delta(t)\right) - \left(1 + \delta(t - t_p)\right) \right\} \times \frac{L_0 k_a}{\kappa} \exp\left(-\frac{2r^2}{\sigma(z)^2}\right) \exp\left(-zk_e\right), \quad (4)$$

where $\delta(t)$ is the Dirac delta function. Hyperbolic equations are associated with waves that have finite propagation speeds that alleviate the physical drawback of diffusion equation. Eq. (4) yields a finite wave speed ($=\sqrt{\alpha/\tau}$) for the propagation speed of the thermal wave. In the limit $\tau \to 0$, Eq. (4) also leads to the parabolic temperature distribution for Fourier case.

In the case of a converging laser beam as used in this paper which is focused at a depth of $z = f_D$, the standard deviation $\sigma(z)$ in Eq. (2) and (4) which varies with z is given as follows:

$$\sigma(z) = \sigma(0)\left(\frac{-(R_0 - R_D)}{R_0}\frac{z}{f_D} + 1\right), \quad 0 \le z \le f_D,$$
$$\sigma(z) = \sigma(0)\left(\frac{(R_0 - R_D)}{R_0}\frac{z}{f_D} - \frac{(R_0 - 2R_D)}{R_0}\right), \quad z > f_D, \quad (5)$$

where $\sigma(0)$ is the standard deviation of radial intensity distribution at the sample surface, R_o is the beam radius at the surface of the sample and R_D is radius of the beam at the focal plane.

The boundary conditions that are used are the following: (i) all the boundaries except the top laser incident surface are insulated, (ii) at the top surface convective heat exchange (convective heat transfer coefficient = 10 W /m^2.K) with surrounding ambient air (25^{0}C) is considered, (iii) the temperature profile is symmetric about the z-axis, and (iv) initially (t = 0) the temperature is equal to the ambient temperature and its derivative with respect time are zero everywhere in space.

For model validation with the tissue phantoms and excised mouse skin tissue samples the effect of convective heat transfer through blood flow is neglected and hence blood perfusion rate (ω_b) is taken as zero. For the case of live anaesthetized mouse the value of ω_b is taken as 7.5 ml/min/100 ml of tissue [25]. The temperature of the blood (T_a) is taken as 30^{0}C. Eq. (4) is discretized to obtain finite difference equations using Alternating Direction Implicit (ADI) scheme with Backward in Time and Central in Space (BTCS) formulation. Details of this discretization scheme and Van Neumann stability analysis can be found in literature [37]. The solutions are obtained by using values of Δr and Δz = 1.5625 x 10^{-4} m and 2.5 x 10^{-5} m respectively and Δt = 25 x 10^{-12} seconds. For hyperbolic case, the value of relaxation time (τ) is taken as 20 seconds for phantoms and 17 seconds for mouse skin tissues. The resultant finite difference equations are solved by Tri-Diagonal Matrix Algorithm (TDMA).

EXPERIMENTAL METHODS

The schematic of the experimental set up is shown in Fig. 1b. A Q-switched short pulse Nd:YAG laser operating at a wavelength of 1064 nm and having a temporal pulse width (t_p) of 200 ns (FWHM) is used in this study. During the experiment the laser power is constantly monitored using a power meter. The samples are well insulated on all sides (except on the irradiated face) to prevent heat loss to the surroundings. A thermal imaging camera (IR Flexcam Pro, Infrared Solutions) is used to record the radial surface temperature profile of the samples. The images are recorded with computerized data acquisition system and processed with National Instruments IMAQ Vision Builder Image processing software. The camera provides a measurement range of 0°C to 350°C with a sensitivity of ±0.09°C at 30°C. The spectral response of the camera is 8 to 14 μm. For the axial temperature measurements in the tissue phantom, holes are drilled up to the central axis at discrete locations along the length of the phantom. T-type

thermocouples having diameter of 0.5 mm are inserted into the holes for temperature measurements. Temperature readings of the thermocouples are recorded through a computerized data acquisition system using Labview Software. These thermocouples provide a measurement range from 0°C to 480°C with a sensitivity of ±1°C and 0.2 seconds of response time.

Experiments are performed on both single-layer and three-layer tissue phantoms replicating skin layers and having an embedded inhomogeneity (Fig. 1a). The phantoms are composed of araldite, DDSA (Dodecenyl Succinic Anhydride) resin and DMP-30 (hardener) mixed in the ratio1:0.87:0.04. Titanium Dioxide particles (mean diameter = 0.3 μm) are added as scatterers to the sample**.** India ink is used as absorber. Details about phantom preparation can be found in the previous papers of the authors [38]. The layered tissue phantom consists of three-layers having different optical properties representing epidermis, dermis, and fatty tissues of human skin. The thickness, absorption coefficient (k_a), and scattering coefficient (k_s) of each layer are tabulated in Table 1.

For single-layer tissue phantom, the base tissue matrix has bulk average absorption coefficient (k_a) = 0.051 mm^{-1}, and scattering coefficient (k_s) = 6.14 mm^{-1}. These values are obtained by calculating weighted average of properties of

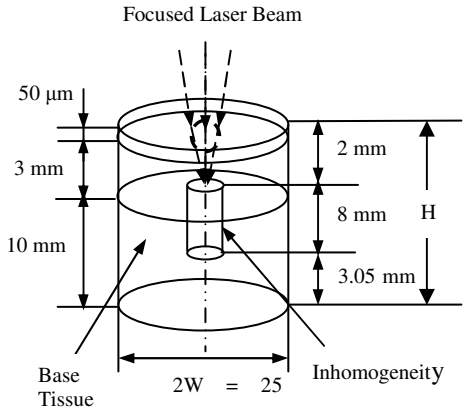

Fig. 1a: Schematic of tissue phantom containing inhomogeneity.

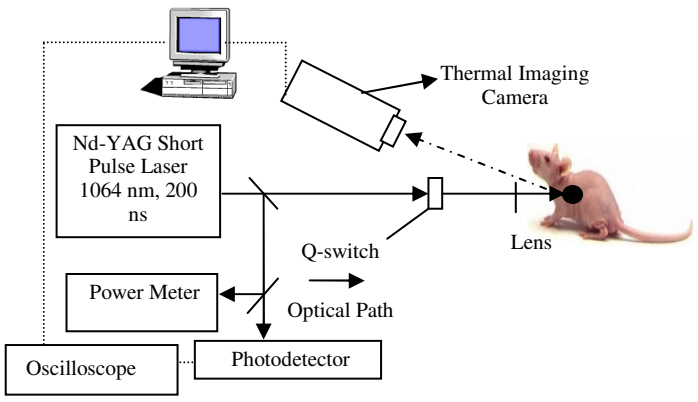

Fig. 1b: Schematic of the experimental set-up for laser irradiation.

Layer	Thickness	Absorption Coefficient (k_a) (mm^{-1})	Scattering Coefficient (k_s) (mm^{-1})
Epidermis	50 μm	0.355	8.237
Dermis	3 mm	0.049	8.237
Fatty tissue	10 mm	0.050	5.5

Table 1: Optical properties of different layers of human skin tissue at 1064 nm [39, 40].

Layer	Thickness	Absorption Coefficient (k_a) (mm^{-1})	Scattering Coefficient (k_s) (mm^{-1})
Epidermis	100 μm	0.7	8.0
Dermis	3 mm	0.044	8.0
Fatty tissue	3 mm	0.04	7.0

Table 2: Optical properties of mouse skin tissue at 1064 nm [41, 42].

layers of layered tissue phantom. The density (ρ) of the medium is 1000 kg/m^3, thermal conductivity (κ) is 0.35 W/m.K, and the specific heat (C_p) is taken as 4200 J/kg.K for all layers of tissue medium [25]. Inhomogeneities are drilled in tissue phantoms and have scattering coefficient of 12.28 mm^{-1} and absorption coefficient of 0.051 mm^{-1}.

Experiments are conducted with freshly excised skin tissue samples with muscle and without muscle which is obtained from mice. Typical tissue cross-section is 20 mm x 30 mm. The density (ρ), thermal conductivity (κ), and specific heat (C_p) are taken as 1000 kg/m^3, 0.35 W/m.K, and 4200 J/kg.K respectively [25]. The density (ρ_b) and the specific heat (C_b) of blood are taken as 1060 kg/m^3 and 3770 J/kg.K respectively [25]. The thickness and optical properties of three different layers of the mouse skin tissues are presented in Table 2.

Finally experiments are conducted with live anaesthetized mouse. Mice of albino trait are anaesthetized using sodium pentobarbital delivered I.P. at a dose of 90 mg/kg. After the experiments, animals are allowed to fully recover before being reintroduced to the animal colony. No signs of stress have been observed before, during or after experimental procedures. All animal experimental procedures are approved by Florida Tech's Institutional Animal Care and Use Committee.

RESULTS AND DISCUSSION

In this paper temperature distribution and heat affected zone are obtained experimentally and numerically for tissue medium irradiated with focused laser beam. Radial and axial temperature distributions are obtained for the case of tissue phantoms, excised skin tissue samples, and live anesthetized mouse. Numerical modeling results are obtained for both hyperbolic non-Fourier and parabolic Fourier case.

Experiments have been first performed on a three-layer tissue phantom containing inhomogeneity using both

collimated and focused laser beam. For the case of focused laser beam, the laser is focused directly at the inhomogeneity location using a converging lens. The sample is irradiated until a prescribed temperature rise of 43^0C is obtained at the focal plane. For both the cases, radial temperature distribution is measured at the laser incident surface (z = 0) and at inhomogeneity location which is 2 mm underneath (z = 2 mm). The surface temperature is measured using thermal camera and the temperature at z = 2 mm is measured using thermocouples. Fig. 2a and Fig. 2b show the comparison of temperature distribution between experimental and numerical modeling results obtained at z = 2 mm at the sample surface respectively. The error bars are plotted in the Fig. 2a and Fig. 2b. Considering a 99% confidence interval, the precision index for a total of three runs is calculated. The standard deviation between the three runs at each individual nodal point is evaluated. Thus the total uncertainty values at each nodal point is the product of the precision index times the standard deviation. It is observed that a maximum total uncertainty of 1.175°C is obtained for thermal camera and 1.515°C for thermocouple. It is observed in both Fig. 2a and Fig. 2b that numerical modeling result obtained from non-Fourier hyperbolic formulation matches extremely well with experimental measurements, where as the traditional Fourier formulation over predicts radial heat spread and under predicts peak temperature rise. It has been observed that the accuracy of prediction provided by hyperbolic heat conduction depends on proper choice of thermal relaxation time (τ). For biological medium such as bologna meat samples the value of τ was found to be of the order of 10-20 seconds [31]. Therefore for the case of tissue phantom the value of τ is taken as 20 seconds. It can also be inferred that for a fixed power considerably higher temperature rise can be obtained at the desired location at a shorter time with smaller heat affected zone using focused beam compared to a collimated beam. Therefore, it is beneficial to use focused beam for applications such as subsurface tumor

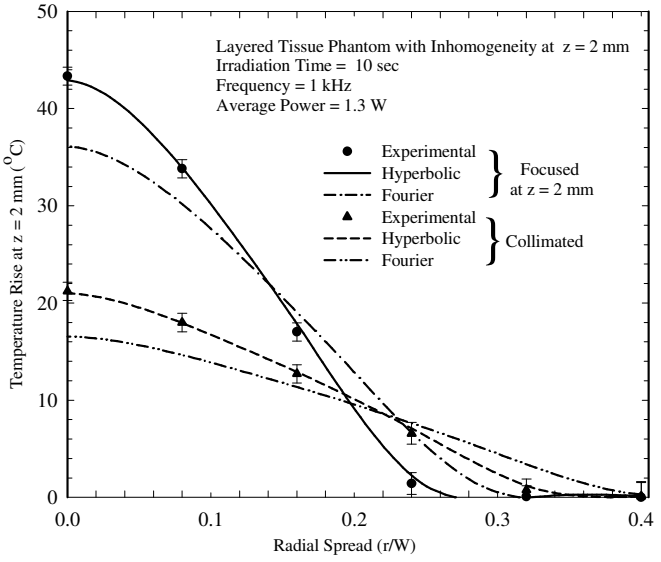

Fig. 2a: Comparison of radial temperature distribution at the inhomogeneity location between collimated and focused laser beam irradiation for a three-layer tissue phantom.

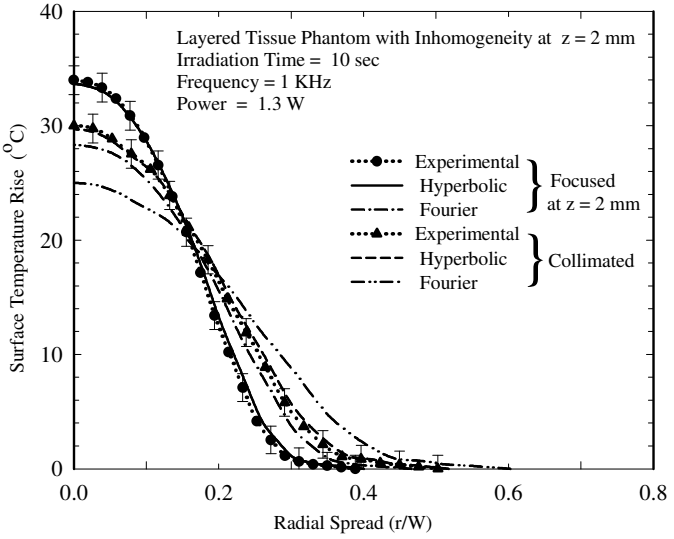

Fig. 2b: Comparison of radial temperature distribution at the surface between collimated and focused laser beam irradiation for a three-layer tissue phantom.

irradiation with minimal damage caused to the surrounding healthy tissues.

After demonstrating the advantage of using focused laser beam and performing model validation studies, experiments are conducted to compare the temperature distribution between a single-layer and three-layer tissue phantom. Conventionally, skin is treated as a single-layer medium for simplicity. But in reality, skin is a multi-layered medium having different thicknesses, scattering, and absorption coefficients. Fig. 3a shows the comparison of the radial temperature distribution at the focal plane (z = 2 mm) between a single-layer and three-layer tissue phantom. Comparison of the experimental measurements with the numerical modeling results demonstrates the validity of hyperbolic heat conduction formulation for analyzing bio-heat transfer phenomenon. It is evident from Fig. 3a that for the case of three-layer tissue phantom, the temperature rise is less but the radial heat spread is slightly more as compared to those of single-layer tissue phantom. These differences can be attributed to the consideration of average optical properties throughout the whole tissue phantom in case of single-layer model. Moreover, axial temperature distribution (Fig. 3b) obtained from thermocouples placed at various depths of the phantom shows lower peak temperature rise (obtained at z = 2 mm) and smaller axial spread for three-layer tissue phantom. This happens due to greater attenuation of laser beam caused by higher absorption coefficient of the first layer of three-layer tissue phantom as compared to single-layer tissue phantom. For both the cases, there is a very good match between experimental and numerical results obtained using hyperbolic heat conduction formulation compared to Fourier formulation. This demonstrates that there is difference in heat affected zone and hence skin must be modeled as a layered medium to analyze bio-heat transport phenomenon.

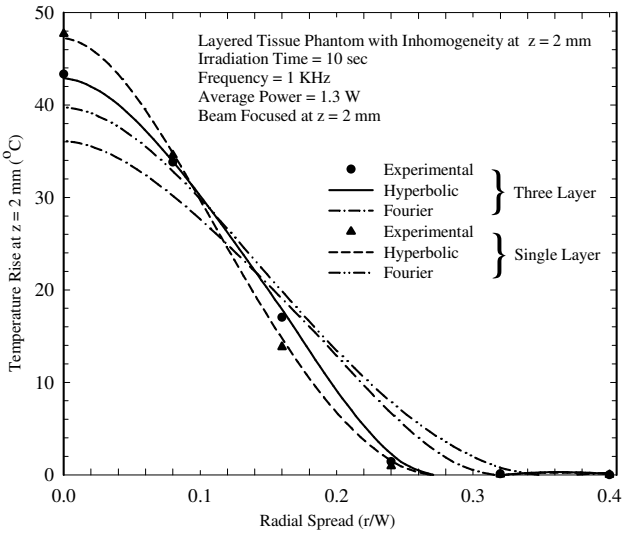

Fig. 3a: Comparison of radial temperature distribution at the inhomogeneity location between a single-layer and a three-layer tissue phantom for focused beam irradiation.

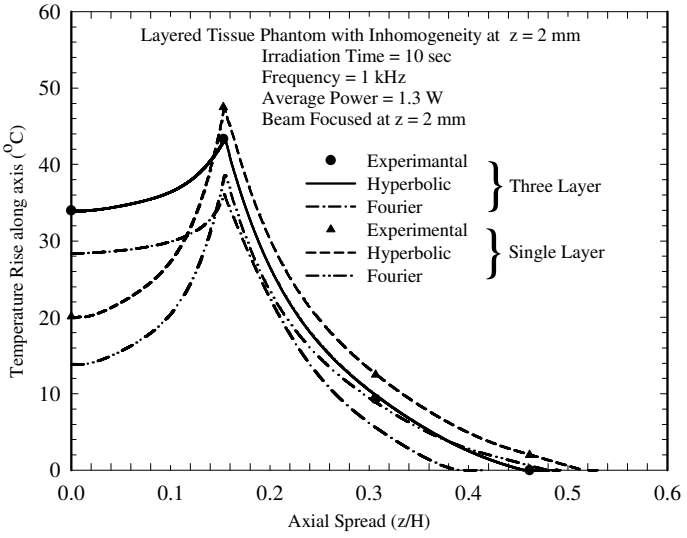

Fig. 3b: Comparison of axial temperature distribution between a single-layer and a three-layer tissue phantom for focused beam irradiation.

After validating the numerical model for the case of tissue phantoms, experiments are further conducted on *in vitro* mouse skin tissue sample. Tissue sample with muscle are irradiated by the laser beam focused at the surface. The temperature distribution at the surface of the tissue is measured using thermal camera. Numerical modeling results are obtained by considering the mouse skin tissue as a three-layer medium. Optical properties as a function of various layers of skin are taken from Table 2. Fig. 4 shows the experimentally measured surface radial temperature distribution along with corresponding numerical results obtained using Fourier parabolic heat conduction and non-Fourier hyperbolic heat conduction formulation for two different power and irradiation

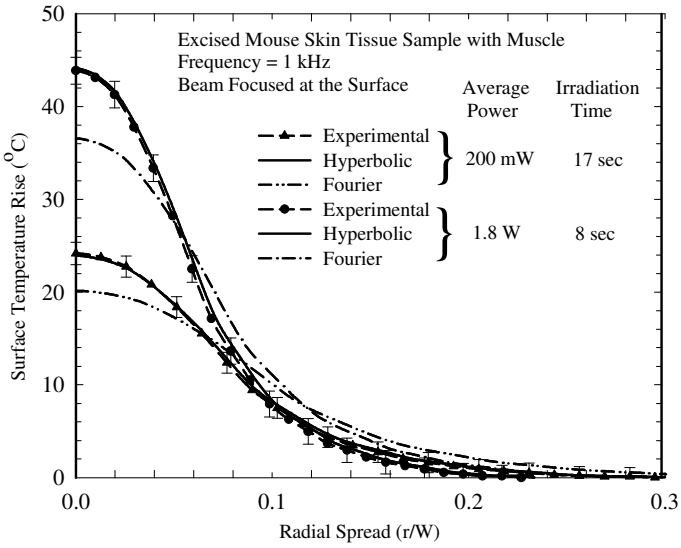

Fig. 4: Surface radial temperature distribution in excised mouse skin tissue sample with muscle for different average powers.

time. Error bars are plotted following the same procedure as previously described. Similar to phantom studies, experimental measurements match extremely well with the results predicted by hyperbolic heat conduction formulation. In this case the value of τ is found to be slightly different (17 seconds) from that obtained for the case of tissue phantom (20 sec). This is expected because the value of τ depends on the propagation velocity of thermal wave which is dependent on material structure and property. These results also emphasize the need to consider tissues as a layered medium to enhance the accuracy of prediction of thermal damage caused by laser irradiation.

It is well known from previous studies that non-Fourier hyperbolic heat conduction phenomenon is important when characteristic time is in the same order of thermal relaxation time of the material. At times larger than relaxation time, both Fourier and non-Fourier heat conduction formulation yields similar result. To demonstrate this effect for the case of tissue samples, mouse skin tissue samples are irradiated with fixed power for different times ranging from 1 second to 50 seconds. Results for only two irradiation times – 8 seconds and 30 seconds are plotted in Fig. 5. It is observed that for small irradiation time of 8 second (shorter than tissue thermal relaxation time) only non-Fourier heat conduction formulation predicts experimental temperature profile accurately. This time corresponds to tissue temperature rise of 43^0C necessary for many therapeutic applications. On the contrary, for higher irradiation times (greater than thermal relaxation time) both Fourier and non-Fourier formulation matches with experimental measurements as expected. Therefore, it is important to consider non-Fourier heat conduction formulation for heat transfer phenomenon occurring at small time scale which is very common in laser-tissue interaction.

After validating the numerical model for tissue phantoms and mouse skin tissue samples, experiments are performed on live anesthetized mouse to analyze bio-heat transfer in presence of blood perfusion. Converging laser beam

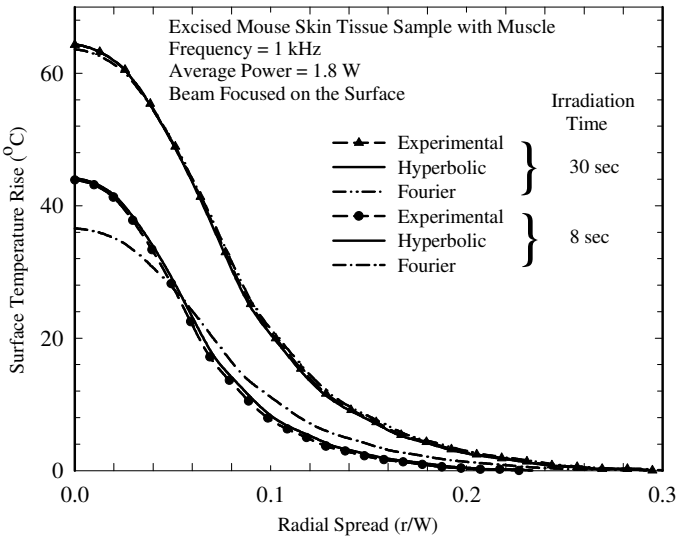

Fig. 5: Surface radial temperature distribution in excised mouse skin tissue sample with muscle for different irradiation times.

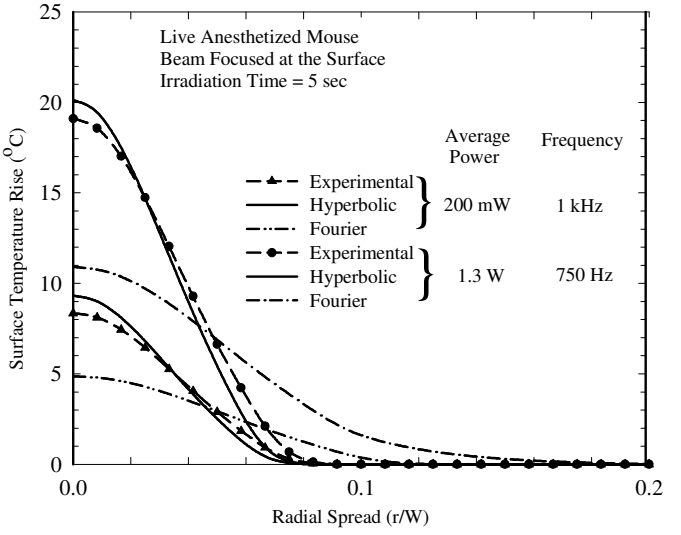

Fig. 6: Surface radial temperature distribution in live anesthetized mouse for different average power and frequency combinations.

is focused underneath the skin surface of a live anesthetized mouse and the temperature distribution at the irradiated spot is measured using thermal camera. In Fig. 6 experimentally measured radial temperature profile at the skin surface is plotted for two different power and frequency combinations for irradiation time of 5 seconds. Corresponding numerical results obtained using Pennes' bio-heat transfer model coupled with either Fourier or non-Fourier heat conduction formulation are also plotted. The irradiation time is less than mouse tissue thermal relaxation time. Hence it is once again observed that non-Fourier formulation is more accurate in predicting temperature profile in live mouse with blood perfusion at short time scales.

CONCLUSION

In this work skin tissue is modeled as a layered medium to analyze heat transfer upon irradiation with a focused laser beam. Temperature distribution and heat affected zones measured experimentally and obtained numerically are compared between single-layer and three-layer tissue phantom model. The radial as well as axial temperature distributions obtained for multi-layer tissue phantoms show a considerable difference between collimated and focused laser beam case. Experimental measurements are compared with numerical modeling results obtained from Fourier parabolic and non-Fourier hyperbolic heat conduction formulation. It is demonstrated that the hyperbolic heat conduction formulation is an accurate model for such kind of analysis as it takes into account the relaxation time of the tissues. Fourier parabolic heat conduction model, on the other hand, is found to under predict the surface temperature rise and over predict the radial heat spread leading to a complete mismatch with the experimental measurements. The importance of considering hyperbolic heat conduction formulation in studying heat transfer phenomenon for a time scale shorter than thermal relaxation time of the medium is also emphasized. Finally, the importance of hyperbolic heat conduction formulation in analyzing the radial spread heat spread is demonstrated for the case of live anesthetized mouse using Pennes' energy balance equation. To the authors' knowledge, this work is the first of its kind in comparing experimental measurements with numerical modeling results for live animal model.

Since the ultimate goal of this research is to develop bio-heat transfer model for laser therapeutic applications such as tumor irradiation, the current work will be extended by comparing the heat affected zone and temperature distribution in live anesthetized mouse with mammary tumors during laser irradiation. Another improvement in current model involves accounting for transient scattering and absorption effects for laser propagation through tissues to obtain the intensity distribution. This would need solving of coupled transient radiative transport equation and Pennes' bio-heat transfer equation to obtain the resulting temperature distribution. This is a challenging task and will be addressed in a future paper.

REFERENCES

[1] Kimel, S., Svaasand, L.O., Kelly, K.M., Nelson, J.S., 2004, "Synergistic photodynamic and photothermal treatment of port-wine stain," *Lasers in Surgery and Medicine*, **34**, pp. 80-82.

[2] Chin, L.C.L., Whelan, W.M., Sherar, M.D., Vitkin, I.A., 2001, "Changes in relative light fluence measured during laser heating: implications for optical monitoring and modeling of interstitial laser photocoagulation," *Physics in Medicine and Biology*, **46**, pp. 2407-2420.

[3] Wahrburg, J., Schmidt, K.U., 1997, "A new system for minimal invasive ablation of deep seated brain tumors," *Proceedings of IEEE/EMBS*, **2438**, pp. 2441.

[4] Schellini, S.A., Brunt, L.F., Hoyama E, Weber, S.A.T., 2004, "Argon laser for treatment of benign eyelid tumors," *Medical Laser Application*, **19**, pp. 114-117.

[5] Mack, M.G., Eichler, K., Straub, R., Lehnert, T., Vogl, T.J., 2004, "MR-guided laser-induced thermotherapy of

head and neck tumors," *Medical Laser Application*, **19**, pp. 91-97.

[6] Chen, W.R., Korbelik, M., Bartels, K.E., Liu, H., Nordquist, R.E., 2004, "Laser immunotherapy: a novel approach for metastatic tumors," *Optical Technologies in Biophysics and Medicine V, Proceedings of SPIE*, **5474**, pp. 25-32.

[7] Kangasniemi, M., McNichols, R.J., Bankson, J.A., Gowda, A., Price, R.E., Hazle, J.D., 2004, "Thermal therapy of canine cerebral tumors using a 980 nm diode laser with MR temperature-sensitive imaging feedback," *Lasers in Surgery and Medicine*, **35**, pp. 41-50.

[8] Manstein, D., Herron, G.S., Sink, R.K., Tanner, H., Anderson, R.R., 2004, "Fractional Photothermolysis: A new concept for cutaneous remodeling using microscopic patterns of thermal injury," *Lasers in Surgery and Medicine*, **34**, pp. 426-438.

[9] Khan, M.H., Sink, R.K., Manstein, D., Eimerl, D., Anderson, R.R., 2005, "Intradermally focused infrared laser pulses: thermal effects at defined tissue depths," *Lasers in Surgery and Medicine*, **36**, pp. 270-280.

[10] Ozturk, S., Hoopman, J., Brown, S.A., Nojima, K., Saboorian, H., Acikel, C., Kenkel, J., 2004, "A useful algorithm for determining fluenece and pulse width for vascular targets using 1,064 nm Nd:YAG laser in animal model," *Lasers in Surgery and Medicine*, **34**, pp. 420-425.

[11] Raskin, B., Fany, R.R., 2004, "Laser treatment for neovascular formation," *Lasers in Surgery and Medicine*, **34**, pp. 189-192.

[12] Gratzl, T., Dohr, G., Schmidt-Kloiber, H., Reichel, E., 1991, "Histological distinction of mechanical and thermal defects produced by nanosecond laser pulses in striated muscle at 1064 nm," *Proceedings of SPIE*, **1427**, pp. 55-62.

[13] Dewhirst, M.W., Viglianti, B.L., Lora-Michiels, M., Hoopes, P.J., Hanson, M., "Thermal dose requirement for tissue effect: Experimental and clinical findings," *Proceedings of SPIE*, **4954**, pp. 37-57.

[14] Arora, D., Skliar, M., Roemer, R.B., 2005, "Minimum-time thermal dose control of thermal therapies," *IEEE Transactions on Biomedical Engineering*, **52**, pp. 191-200.

[15] Bagley, D.H., 1998, "Ureteroscopic laser treatment of upper urinary tract tumors," *Journal of Clinical Laser Medicine and Surgery*, **16**, pp. 55-59.

[16] Pennes, H.H., 1948, "Analysis of tissue and arterial blood temperatures in resting forearm," *Journal of Applied Physiology*, **1**, pp. 93-122.

[17] Weinbaum, S., Jiji, L.M., 1985, "A new simplified bioheat equation for the effect of blood flow on local average tissue temperature, *ASME Journal of Biomechanical Engineering*, **107**, pp. 131-139.

[18] Zhu, M., Weinbaum, S., Jiji, L.M., Lemons, D.E., 1988, "On the generalization of the Weinbaum-Jiji bioheat equation to microvessels of unequal size; the relation between the near field and local average tissue temperatures," *ASME Journal of Biomechanical Engineering*, **110**, pp. 75-81.

[19] Arkin, H., Holmes, K.R., Chen, M.M., 1987, "Theory on thermal probe arrays for the distinction between the convective and the perfusive modalities of heat transfer in living tissues," *ASME Journal of Biomechanical Engineering*, **109**, pp. 346-352.

[20] Baish, J.W., Cheevers, E., 1988, "An isotropic thermal phantom of perfused tissue," *Proceedings of IEEE*, **2666**, 126-129.

[21] Xu, L.X., Holmes, K.R., Moore, B., Chen, M.M., and Arkin, H., 1994, "Microvascular architecture with in the pig kidney cortex," *Microvascular Resources*, **47**, pp. 293-307.

[22] Zhu, L., 2000, "Theoretical evaluation of contributions of heat conduction and counter-current heat exchange in selective brain cooling in humans," *Annals of Biomedical Engineering*, **28**, pp. 269-277.

[23] Shrivastava, D., McKay, B., Roemer, R.B., 2005, "An analytical study of heat transfer in finite tissue with two blood vessels and uniform Dirichlet boundary condition," *ASME Journal of Heat Transfer*, **127**, pp. 179-188.

[24] Rai, K.N., Rai, S.K., 1999, "Effect of metabolic heat generation and blood perfusion on the heat transfer in the tissues with a blood vessels," *Heat and Mass Transfer*, **35**, pp. 75-79.

[25] Liu, J., Chen, X., Xu, L.X., 1999, "New thermal wave aspects on burn evaluation of skin subjected to instantaneous heating," *IEEE Transactions on Biomedical Engineering*, **46**, pp. 420-428.

[26] Deng, Z., Liu, J., 2003, "Non-Fourier heat conduction effect on prediction of transients and thermal stress in skin cryopreservation", *Journal of Thermal Stresses*, **26**, pp. 779-798.

[27] Charny, C.K., Levin R.L., 1989, "Bioheat transfer in a branching countercurrent network during hyperthermia," *ASME Journal of Biomechanical Engineering - Trans. ASME*, **111**, pp. 263-270.

[28] Jou, D., Casas-Vázquez, J., Lebon, G., 1988, "Extended irreversible thermodynamics," *Report on Progressive Physsics*, **51**, pp. 1105-1179.

[29] Tzou, D. Y., 1993, "An engineering assessment to the relaxation time in thermal waves," *International Journal of Heat and Mass Transfer*, **36**, pp. 1845-1851.

[30] Ozisik, M.N., Tzou, D.Y., 1994, "On the wave theory of heat conduction," *ASME Journal of Heat Transfer*, **116**, 526-535.

[31] Mitra, K., Kumar S., Vedavarz, A, Moallemi, M.K., 1995, "Experimental evidence of hyperbolic heat conduction in processed meat," *ASME Journal of Heat Transfer*, **117**, pp. 568-573.

[32] Kaminski, W., 1990, "Hyperbolic heat conduction equation for materials with a nonhomogenous inner structure," *ASME Journal Heat Transfer*, **112**, pp. 555-560.

[33] Vedavarz, A., Mitra, K., Kumar S., 1994, "Hyperbolic temperature profiles for laser surface interactions," *Journal of Applied Physics*, **76**, pp. 5014-5021.

[34] Banerjee, A., Ogale, A., Das, C., Mitra, K., Subramanian, C., 2005, "Temperature distribution in different materials," *ASME Journal of. Heat Transfer Engineering*, **26**, pp. 41-49.

[35] Tzou, D.Y., 1996, "Macro to micro heat transfer," Taylor and Francis, Washington DC.

[36] Antaki, P.J., 2005, "New interpretation of non-Fourier heat conduction in processed meat, *ASME Journal Heat Transfer*, **127**, pp. 189-193.
[37] Tanehill, J.C., Anderson, D.A., Pletcher, R.H., 1984, "Computational fluid mechanics and heat transfer, 2nd edition, Washington DC: Taylor and Francis, Chapter 4.
[38] Das, C., Trivedi, A., Mitra, K., Vo-Dinh, T., 2003, "Experimental and numerical analysis of short pulse laser interaction with tissue phantoms containing inhomogeneities, *Applied Optics*, **42**, pp. 5173-5180.
[39] Djorev, P.L, Borisova, E., Avramov, L., 2003, "Interaction of the IR laser radiation with human skin - Monte-Carlo simulation," *Proceedings of SPIE - The International Society for Optical Engineering*, **5226**, pp. 403-407.
[40] Simpson, R.C., Kohl, M., Essenpreis, M., Cope, M., 1998, "Near-infrared optical properties of ex vivo human skin and subcutaneous tissues measured using the Monte Carlo inversion technique," *Physics in Medicine and Biology*, **43**, pp. 2465-2478.
[41] Jacques, S.L., 1998, "Skin optics," Oregon Medical Laser Center News.
[42] Nilsson, A.M.K., Berg, R., Andersson-Engels, S., 1995, "Measurements of the optical properties of tissue in conjunction with photodynamic therapy," *Applied Optics*, **34**, pp. 4609-4619.